PAPER • OPEN ACCESS

Laser photoexcitation of Rydberg states in helium with $n > 400$

To cite this article: S D Hogan *et al* 2018 *J. Phys. B: At. Mol. Opt. Phys.* **51** 145002

View the article online for updates and enhancements.

Laser photoexcitation of Rydberg states in helium with $n > 400$

S D Hogan[iD], Y Houston and B Wei

Department of Physics and Astronomy, University College London, Gower Street, London WC1E 6BT,
United Kingdom

E-mail: s.hogan@ucl.ac.uk

Abstract
Helium atoms travelling in pulsed supersonic beams have been photoexcited from the metastable $1s2s\,^3S_1$ level to Rydberg states with principal quantum numbers exceeding 400 by resonance-enhanced two-colour two-photon excitation using narrow-bandwidth CW laser radiation. To achieve this, the photoexcitation region was shielded and stray electric fields cancelled using a cubic arrangement of 80 mm $\times$ 80 mm copper plates. The excited Rydberg atoms were detected by pulsed electric field ionisation downstream from this photoexcitation region. Comparison of the experimental spectra with the results of calculations indicate that the stray electric fields at the position of Rydberg state photoexcitation were reduced to as low as 160 μV cm^{-1}. Using helium in these experiments minimises temporal changes in the stray fields resulting from surface adsorption. Measurements performed 70 h apart indicate that the rate of change of these fields was on the order of 2 μV cm^{-1} per h, making beams of metastable helium atoms ideally suited as probes for high precision electrometry in spectroscopy experiments involving less readily available species such as positronium or antihydrogen.

Keywords: Rydberg states, electric fields, helium

(Some figures may appear in colour only in the online journal)

1. Introduction

The large static electric dipole polarisabilities, static electric dipole moments and electric dipole transition moments associated with high Rydberg states of atoms and molecules [1] make samples in these states very sensitive probes of static [2–7] and time-dependent electric fields [8–13]. Because of this sensitivity it is also therefore essential to carefully control or cancel these fields when performing experiments with Rydberg atoms and molecules. This is particularly true when coherent interactions with narrow-bandwidth electromagnetic fields over long timescales are required for precision spectroscopy [14–17] or quantum information processing, see, e.g., [18] and references therein.

Interest in performing precision spectroscopic studies of Rydberg states of exotic species such as antihydrogen or positronium, with a view to probing matter–antimatter assymmetries [17, 34], and contributing to the resolution of the current puzzle relating to the proton charge radius as determined in precision spectroscopic studies of atomic hydrogen and muonic hydrogen [19–22] makes it desirable to identify appropriate off-line methods for the characterisation and cancellation of stray electric and magnetic fields in these experimental settings. The exceptional sensitivity of high Rydberg states to these fields makes them ideal probes of these environments with the optimal cancellation of stray electric fields achieved in experiments in which the highest Rydberg states are photoexcited. In the past, precise cancellation of stray laboratory electric fields and studies of very high n Rydberg states have been performed using beams of alkaline earth metal atoms. Rydberg states with principal quantum numbers exceeding $n = 500$ have been resolved in laser photoexcitation spectra of barium [2] and strontium [23]. These atoms are well suited to the photoexcitation of such
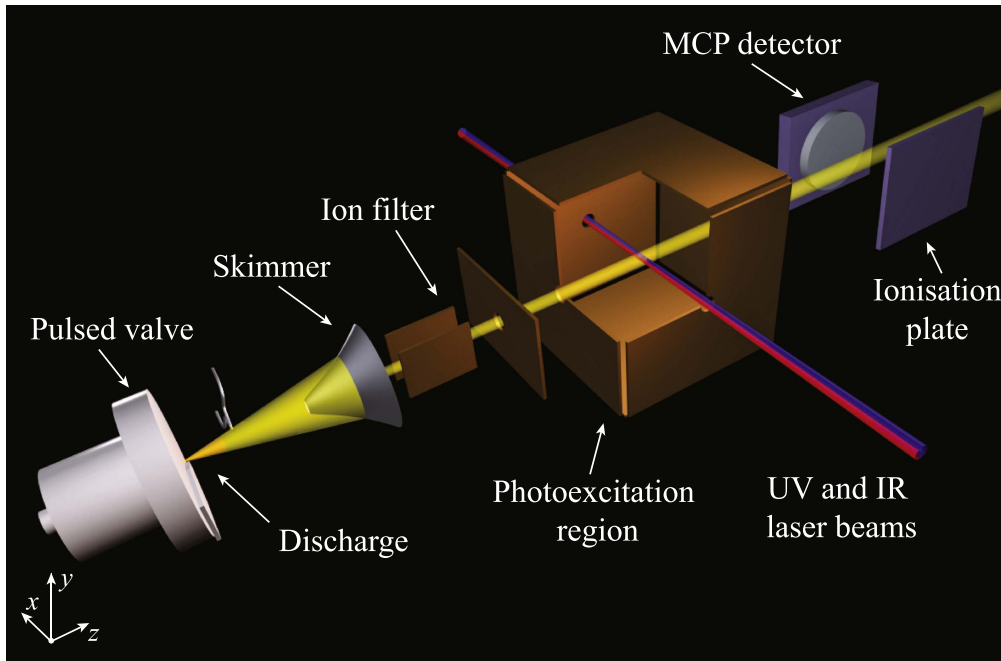
Figure 1. Schematic diagram of the experimental apparatus.

high Rydberg states, and hence sensitive measurements of, and applications in the cancellation of, weak static electric fields because of the large oscillator strength for transitions from low-n intermediate $^1P_1$ levels to high-n $^1D_2$ Rydberg levels. However, because of their large ground-state static electric dipole polarizabilities of $\alpha_{Ba} \sim 270$ au and $\alpha_{Sr} \sim 190$ au [24] (1 au = $1.648\,773 \times 10^{-41}$ C m^2 V^{-1}), these atoms are prone to cause time-dependent changes in stray electric fields following surface adsorption. In cryogenic environments, in which antihydrogen atoms are synthesised and precision spectroscopy of high Rydberg states must be carried out to minimise contributions from blackbody radiation, these effects are expected to be even more pronounced than in experiments performed at room temperature.

To perform sensitive electrometry with minimal contamination of the apparatus, or contributions to time-dependent changes in stray fields following surface adsorption, beams of rare gas atoms are most suitable. Studies of very high n Rydberg states of argon and krypton, in which precise electric field cancellation was implemented, have been performed previously [4, 25–27]. The ground-state static electric dipole polarizabilities of these atoms are $\alpha_{Ar} \sim 10.77$ au and $\alpha_{Sr} \sim 16.47$ au, respectively [28]. Consequently, effects of time-dependent changes in stray electric fields following surface adsorption are likely to be significantly smaller than in experiments with Ba or Sr. However, in cryogenic environments, i.e., in apparatus operated at temperatures on the order of 10 K and below, these heavier rare gas atoms are prone to freeze onto electrode surfaces. This can lead to the accumulation of insulating patches on these metallic surfaces where charge build up can occur and act as a further source of time-dependent stray electric fields. To avoid these problems, helium atoms are optimal for sensitive electrometry in cryogenic environments [29]. By using helium in such settings

surface adsorption within the apparatus is low, even in cryogenic environments. This, together with the low ground-state static electric dipole polarizability of helium of $\alpha_{He} \sim 1.38$ au [28], ensures that contributions from the atoms to time-dependent changes in stray fields are minimised.

Direct laser photoexcitation of Rydberg states in helium at high spectral resolution from the ground state is difficult because of the short wavelength radiation required to achieve this. However, as demonstrated here, population of the metastable 1s2s $^3S_1$ level in an electric discharge, allows subsequent high-resolution resonance-enhanced two-colour two-photon CW laser photoexcitation of Rydberg states with values of $n > 400$. By exploiting these highly excited Rydberg states as sensitive probes of static electric fields in the experimental apparatus, these fields have been cancelled to 160 μV cm^{-1} with a sensitivity of better than ± 20 μV cm^{-1}.

In the following, the apparatus in which the experiments were performed is first described. Laser photoexcitation spectra extending to Rydberg states with $n > 400$ are then presented. Comparison of these measured spectra with spectra calculated for a range of weak electric fields are then made to allow residual stray static electric fields to be characterised, and bounds to be placed on the time-dependence of changes that occur in these fields.

2. Experiment

A schematic diagram of the apparatus used in the experiments is presented in figure 1. A pulsed supersonic beam ($\bar{v}_z \simeq 2\,000$ m s^{-1}) of helium atoms in the metastable 1s2s $^3S_1$ level was generated in an electric discharge at the exit of a pulsed valve [30]. The valve was operated at a repetition rate of 50 Hz. After passing through a 2 mm diameter skimmer and

electrostatic ion filter, to remove charged particles emanating from the discharge, the atomic beam entered the central laser photoexcitation region of the apparatus which was maintained at a background pressure of 10^{-8} mbar. This region was located within a 80 mm × 80 mm × 80 mm cubic structure composed of three pairs of parallel copper plates. The design of this shielded photoexcitation region is based on that used by Frey *et al* [3] and Ye *et al* [23] in experiments to study high-n Rydberg states of potassium and strontium, respectively. The atomic beam entered (exited) the photoexcitation region through a 3 mm diameter (6 mm diameter) aperture in the copper plate oriented parallel to the xy plane and located closest (furthest) from the beam source. The UV (25708.588 cm^{-1} ≡ $388.975\,08$ nm) and IR (tuned between $12\,735$ cm^{-1} ≡ 785.230 nm and $12\,746$ cm^{-1} ≡ 784.584 nm) CW laser radiation used to drive each step of the resonance-enhanced two-colour two-photon $1s2s\,{}^{3}S_1 \rightarrow 1s3p\,{}^{3}P_2 \rightarrow 1snd\,{}^{3}D$ Rydberg state excitation scheme, respectively, entered and exited the photoexcitation region through 3 mm diameter apertures in the center of the copper plates oriented parallel to the zy plane. From previous studies of static electric dipole interactions in ensembles of excited Rydberg atoms [31], the density of helium atoms in the metastable $1s2s\,{}^{3}S_1$ level in the photoexcitation region of the apparatus is estimated to be $<10^8$ cm^{-3}. The typical density of Rydberg atoms in states with values of $n > 275$ is below 10^5 cm^{-3}. Even for these high values of n, the corresponding frequency shifts associated with electric dipole–dipole interactions between excited atoms at these densities (typically 1–10 MHz) are below the spectral resolution of the apparatus. After interacting with the laser radiation, the high longitudinal speed of the atomic beam allowed for the excited atoms to exit the photoexcitation region and be detected by pulsed electric field ionisation upon the application of a pulsed potential of -550 V to the ionisation plate indicated in figure 1. The resulting electrons were then collected at a microchannel plate detector. Separating the photoexcitation and detection regions in the apparatus in this way minimised effects of electric field noise in the excitation region caused by the process of switching the ionisation electric fields.

The electric fields at the position where the focussed laser beams interacted with the atomic beam at the center of the photoexcitation region were controlled by applying individual dc electric potentials to each of the six copper plates. To further minimise effects of electrical noise, to which high Rydberg states with large static electric dipole moments are particularly sensitive [10, 11], the potential applied to each electrode was generated using a 1.5 V battery and an adjustable potential divider. Inside the vacuum chamber in which the experiments were performed, the wires used to apply these potentials to each pair of parallel copper plates surrounding the photoexcitation region were wound as a twisted pair.

3. Results

Using narrow-bandwidth CW laser systems, the selective laser photoexcitation of individual very high Rydberg states of
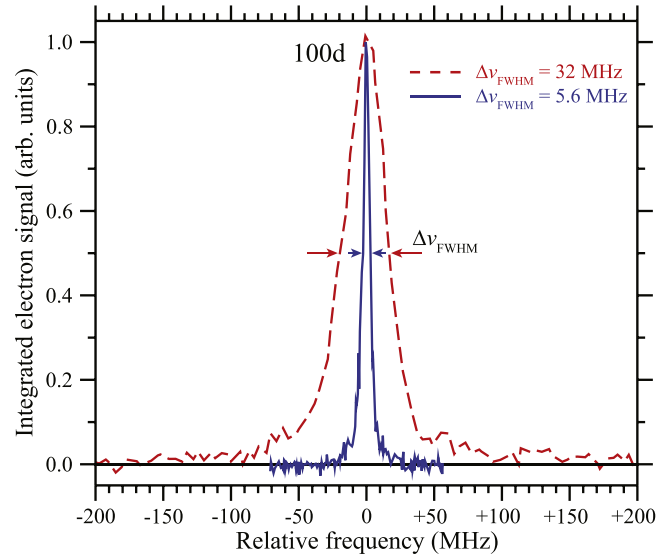

Figure 2. Laser spectrum of the $1s3p\,{}^{3}P_2 \rightarrow 1s100d\,{}^{3}D$ transition in helium recorded with the photoexcitation laser beams unfocussed (continuous blue curve for which $\Delta\nu_{\mathrm{FWHM}} = 5.6$ MHz ≡ $0.000\,187$ cm^{-1}) and focussed (dashed red curve for which $\Delta\nu_{\mathrm{FWHM}} = 32$ MHz ≡ $0.001\,067$ cm^{-1}).

atoms or molecules is in general not limited by the spectral resolution of laser radiation but instead by uncontrolled stray external fields at the photoexcitation position. In the experiments reported here the maximal achievable resolution is limited by the finite fluorescence lifetime of the intermediate $1s3p\,{}^{3}P_2$ level, $\tau_{1s3p\,{}^{3}P_2} \simeq 95$ ns [32]. As can be seen from the spectrum of the $1s3p\,{}^{3}P_2 \rightarrow 1s100d\,{}^{3}D$ transition in figure 2 (continuous blue curve), this, combined with contributions from uncertainties in laser frequency stabilisation and Doppler broadening, yields a spectral resolution of $0.000\,187$ cm^{-1} (≡5.6 MHz). When recording this spectrum the laser beams were not focussed. The corresponding full-widths-at-half-maximum (FWHM) of their Gaussian spatial profiles in the z dimension was ∼0.7 mm, and the interrogation time of the atoms by the laser radiation was therefore ∼350 ns, i.e., 3.7 times the fluorescence lifetime of the intermediate $1s3p\,{}^{3}P_2$ level. Consequently, the spectral resolution was not limited by this finite interrogation time. Because of the very small electric dipole moments, $d_{3p,nd}$, for transitions from this intermediate level to very high Rydberg states, e.g., $d_{3p,400d} = 0.001\,2\,e\,a_0$, it was necessary to focus the laser beams to FWHM beam waists of $\lesssim 100$ μm to ensure a sufficient rate of production of excited states in the experiments. The reduced interaction time of the atoms with the laser beams under these conditions resulted in an increased spectral width of $0.001\,07$ cm^{-1} (≡32 MHz) as can be seen from the corresponding spectrum of the $1s3p\,{}^{3}P_2 \rightarrow 1s100d\,{}^{3}D$ transition indicated by the dashed red curve in figure 2. In the experiments described in the following this is the effective spectral resolution. This spectral width is equal to the interval between Rydberg states in helium with principal quantum numbers 590 and 591 in the absence of external fields.

The spectra in figure 2 were recorded after minimising the stray electric fields in the photoexcitation region of
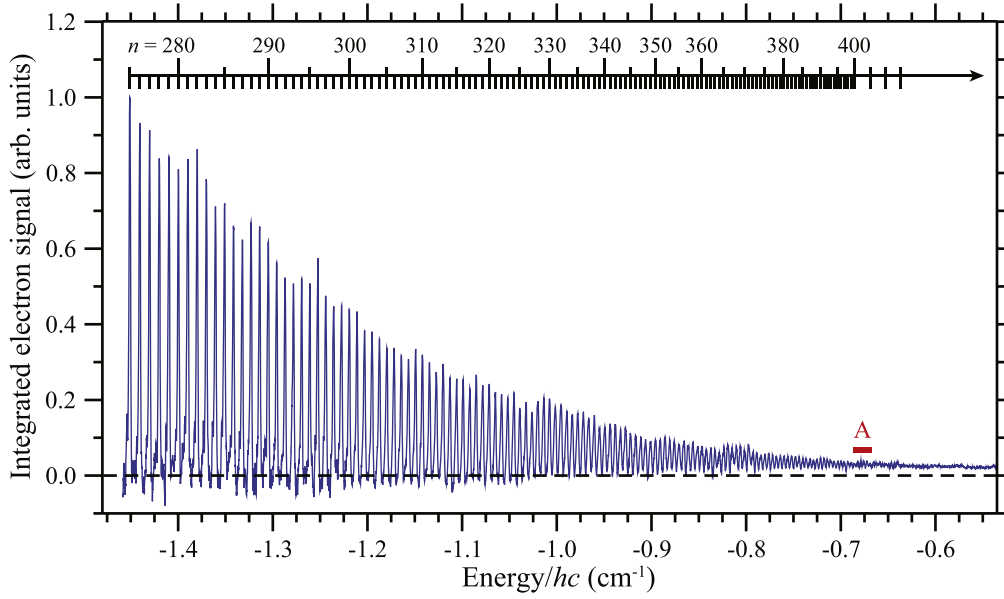
Figure 3. Laser spectrum of the 1s3p ³P₂ → 1snd ³D transitions in helium for values of *n* ranging from 275 to *n* ≃ 450. An expanded view of the spectral region around *n* = 400, as indicated by the horizontal red bar labelled A, is displayed in figure 4.

the apparatus by repeated sequential adjustment of the offset potentials applied to the pairs of electrodes in the *xy*, *xz* and *yz* planes. To achieve this, laser spectra of the 1s3p ³P₂ → 1s100d ³D transition were recorded for each applied cancellation field and the quadratic Stark energy shift of the 1s100d ³D levels was minimised. Using this procedure the stray electric field at the position of Rydberg state photoexcitation was cancelled to $\sim\pm 1$ mV cm^{-1}. Further field cancellation required the excitation of higher Rydberg states which acted as more sensitive probes of the residual stray field. Spectra were therefore subsequently recorded of transitions to states in the vicinity of *n* = 200. This allowed the stray fields to be more accurately cancelled by minimising the spectral width of the manifold of Stark states with linear Stark energy shifts associated with each value of *n*. This process was then repeated for states between *n* = 250 and 400 in intervals of approximately 50. Upon completion of this stray field cancellation procedure spectra encompassing transitions to a wide range of these very high *n* Rydberg states were recorded. The IR laser system used to drive the 1s3p ³P₂ → 1snd ³D transitions could be continuously tuned, mode-hop free, over a spectral range of 0.66 cm^{-1} (≡20 GHz). Therefore the spectrum presented in figure 3, which includes transitions to Rydberg states with values of *n* from 275 to the wavenumber associated with the transition to states with *n* ≃ 450, was recorded in several sections, each covering the transitions to approximately 50 Rydberg states. In this spectrum, the shoulder on the low wavenumber side of the features with values of *n* between 275 and 300 corresponds to the transition to the 1sns ³S₁ level which has a quantum defect of 0.296 657 [33]. Individual Rydberg states can be distinguished up to *n* ∼ 420 (see, e.g., figure 4).

From the spectrum in figure 3 the residual uncancelled stray electric field could be determined most precisely by studying the region encompassing the transitions to states

with values of *n* close to 400 and indicated by the horizontal red bar labelled A. The corresponding portion of the experimentally recorded spectrum, displayed in figure 4, was compared to the results of calculations over the same spectral region performed for a range of trial electric fields, *F*. These spectra were calculated by considering the linear Stark energy shifts, $E^{\text{Stark}}_{|n\,n_1\,n_2\,m_\ell\rangle}$, of the ℓ-mixed hydrogenic Stark states in helium,

$$E^{\text{Stark}}_{|n\,n_1\,n_2\,m_\ell\rangle} = \frac{3}{2}n(n_1 - n_2)ea_{\text{He}}\,F, \quad (1)$$

where n_1 and n_2 are the parabolic quantum numbers, *e* is the charge of the electron, $a_{\text{He}} = a_0\, m_e/\mu_{\text{He}}$ is the Bohr radius corrected for μ_{He}, the reduced mass of helium. For each value of the azimuthal quantum number m_ℓ, the allowed values of $n_1 - n_2$, the difference between the parabolic quantum numbers, range from $-(n - |m_\ell| - 1)$ to $+(n - |m_\ell| - 1)$ in intervals of 2. The relative spectral intensity of the transition from the 1s3p ³P₂ level to each $|n\,n_1\,n_2\,m_\ell\rangle$ Stark state was determined from the squares of the transformation coefficients from the parabolic $|n\,n_1\,n_2\,m_\ell\rangle$ basis to the spherical $|n\,\ell\,m_\ell\rangle$ basis which can be expressed in terms of Wigner-3J symbols as [1]

$$\langle n\,n_1\,n_2\,m_\ell|n\,\ell\,m_\ell\rangle = (-1)^{[(1-n+m_\ell+n_1-n_2)/2]+\ell}$$

$$\times \sqrt{2\ell + 1}\begin{pmatrix} \dfrac{n-1}{2} & \dfrac{n-1}{2} & \ell \\ \dfrac{m_\ell + n_1 - n_2}{2} & \dfrac{m_\ell - n_1 + n_2}{2} & -m_\ell \end{pmatrix} \quad (2)$$

such that

$$|n\,n_1\,n_2\,m_\ell\rangle = \sum_\ell |n\,\ell\,m_\ell\rangle\langle n\,\ell\,m_\ell|n\,n_1\,n_2\,m_\ell\rangle. \quad (3)$$

In the calculation each spectral feature was convoluted with a Lorentzian spectral profile with a FWHM of 0.001 07 cm^{-1}
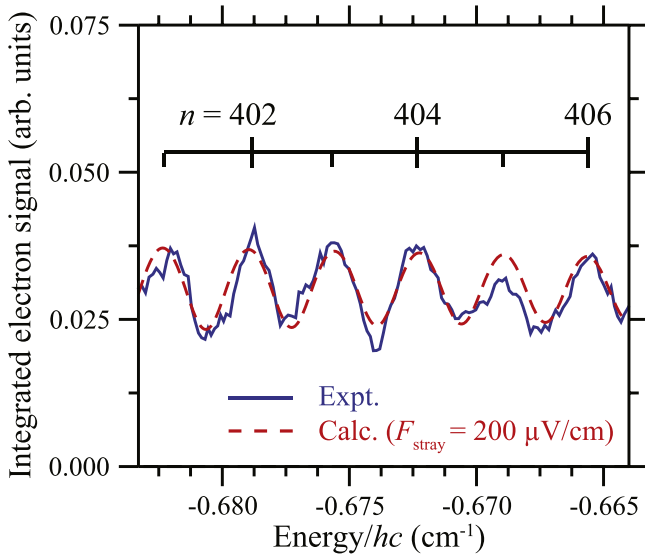
Figure 4. Expanded view of the spectral region encompassing Rydberg states with values of *n* between 401 and 406 as indicated by the horizontal red bar labelled A in figure 3. Comparison of the experimental data (continuous blue curve) with the results of calculations (dashed red curve) indicates that the spectral broadening in the measurements is commensurate with the presence of an uncancelled stray electric field in the photoexcitation region of the apparatus of $\sim$200 μV cm^{-1}.

Figure 5. Laser spectra encompassing transitions to Rydberg states with values of *n* between 373 and 375. The spectrum indicated by the continuous red curve was recorded approximately 70 h after that indicated by the dashed blue curve (see text for details). The experimental data are compared with the results of calculations for fields of 210 $\pm$ 50 μV cm^{-1} (shaded gray region).

($\equiv$32 MHz) as determined from the data in figure 2. This approach to considering the Stark energy shifts and relative spectral intensities of the hydrogenic Stark states is applicable under the conditions of the experiments because the parallel linear polarisations of the UV and IR laser beams result in the predominant photoexcitation of *n*d Rydberg states with $|m_\ell| = 2$. The quantum defect of the *n*d Rydberg states is 0.0029 [33]. Consequently, these states, and those with values of $\ell > 2$ are close to degenerate in zero electric field. In fields close to the Inglis–Teller limit [1], in which the Stark manifolds with values of *n* which differ by +1 cross, the Stark energy shifts of these states, and spectral intensity distributions are indistinguishable from those in a hydrogen atom. The dashed red curve in figure 4, overlaid on the experimental data (continuous blue curve), was calculated for a residual uncancelled electric field of 200 μV cm^{-1}. The good agreement of this calculated spectrum with the experimental data leads to the conclusion that stray electric fields in the apparatus were cancelled to this level when the spectrum was recorded.

The advantages of using helium atoms for precise electrometry center upon the minimal disturbances they cause to the surrounding environment in the experimental apparatus following surface adsorption. Bounds can be placed on the time-dependent changes in the residual uncancelled stray electric fields in the apparatus used here following repeated measurements performed at the same values of *n* without changing the offset potentials applied to the electrodes surrounding the photoexcitation region. The results of such measurements, for values of *n* between 373 and 375 are displayed in figure 5. The experimental spectra in this figure are
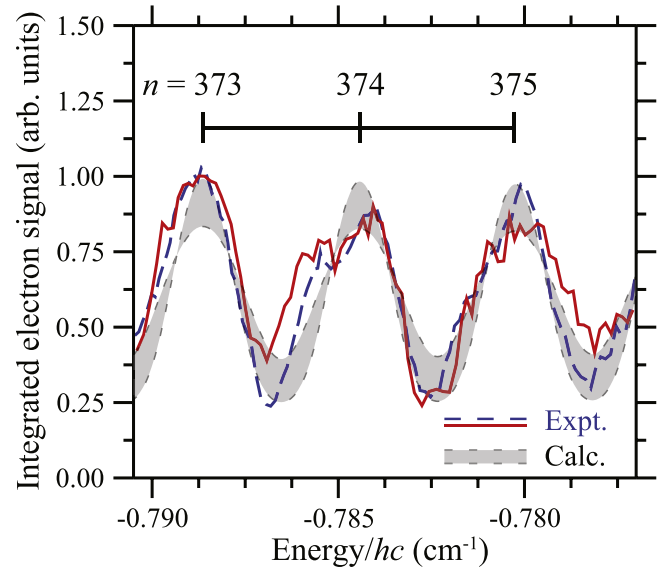
indicated by the dashed blue, and continuous red curves. The data-point–to–data-point fluctuations are greater in the latter spectrum because of a slightly reduced averaging time for each measurement. These spectra were recorded approximately 70 h apart with the data indicated by the dashed blue curve recorded first. During this time the metastable helium beam was operating for approximately 5 h. The changes in the magnitude of the residual uncancelled stray electric fields between the two measurements are determined by comparison of the experimental data with the spectra calculated for fields of 210 $\pm$ 50 μV cm^{-1} as indicated by the shaded gray region in the figure. The bounds of this shaded region with the higher (lower) contrast correspond to the results of the calculations for fields of 160 μV cm^{-1} (260 μV cm^{-1}). From this data the contrast of the spectral features in the dashed blue spectrum indicates the presence of a residual stray electric field with a magnitude close to that at the lower end of the calculated range, i.e., $\sim$160 μV cm^{-1}. On the other hand, the spectrum recorded 70 h later matches more closely that corresponding to a residual field of $\sim$260 μV cm^{-1}. Under the assumption that collisions of helium atoms with, and adsorption on, the surfaces of the copper plates surrounding the photoexcitation region do not significantly affect these stray fields, it can be concluded that the stray fields in the apparatus drift at a rate of $\sim$2 μV cm^{-1} h^{-1}, dominated by surface adsorption of the background gas in the unbaked vacuum chamber. Collisions of helium atoms in the metastable 1s2s ^{3}S$_1$ level with the copper electrodes surrounding the Rydberg state photoexcitation region, or with the background gas—leading to Penning ionisation—do not appear to contribute significantly to changes in the stray electric fields in the these experiments. The dexcitation of a metastable helium atom, or the

J. Phys. B: At. Mol. Opt. Phys. **51** (2018) 145002

S D Hogan *et al*

neutralisation of a Penning ionised atom or molecule from the background gas, on one of the copper surfaces may be expected, as a first approximation, to have a similar effect on the stray electric fields as the adsorption of a ground-state helium atom, or neutral atom or molecule from the background gas. This situation would of course be different in collisions of the metastable helium atoms, or ionised components of the background gas, with the insulating spacers used to position the copper electrodes. However, in the construction of the electrode structure surrounding the photoexcitation region, particular care was take to avoid all direct lines of sight from the position at which the laser beams crossed the atomic beam to these insulating spacers.

4. Conclusion

In conclusion, we report for first time spectra of very high Rydberg states of helium with values of $n > 400$. These highly excited states are bound by < 0.7 cm^{-1} ($\equiv 21$ GHz $\equiv 90$ μeV). The expectation value of the position operator associated with the Rydberg electron, e.g., $\langle r_{n=400} \rangle$, and hence the spatial extent of the Rydberg electron wavefunction in these states is ~ 13 μm. As such, helium atoms in these excited states are truly macroscopic objects with static electric dipole moments of up to 610 000 D. The sensitivity of these electric dipoles to static electric fields has been exploited for precise electrometry allowing the cancellation of stray electric fields within our experimental apparatus to as low as ~ 160 μV cm^{-1}. We expect that these fields can be further reduced in the future with improved preparation of the copper surfaces surrounding the photoexcitation region and the implementation of further methods to reduce low-frequency time-dependent electric field noise. We have shown that using helium atoms in this work results in time-dependent changes in residual uncancelled stray fields on the order of 2 μV cm^{-1} h^{-1}. These results demonstrate that precise electrometry in which helium atoms are employed as the probe may be transferred to other settings, e.g., experiments involving Rydberg positronium or antihydrogen, where contamination of the experimental environment with other more reactive species, such as alkaline earth metal atoms would be extremely detrimental. Laser photoexcitation and detection of atoms in these very high Rydberg states in spatially separated locations was facilitated in part by the high longitudinal speed of the supersonic beams of helium. This approach could also be adopted in using very high Rydberg states of helium for electrometry in these other settings.

Acknowledgments

ORCID iDs

S D Hogan ● https://orcid.org/0000-0002-7720-3979

References

[1] Gallagher T F 1994 *Rydberg Atoms* (Cambridge: Cambridge University Press)

[2] Neukammer J, Rinneberg H, Vietzke K, König A, Hieronymus H, Kohl M, Grabka H-J and Wunner G 1987 Spectroscopy of Rydberg atoms at $n \simeq 500$: observation of quasi-Landau resonances in low magnetic fields *Phys. Rev. Lett.* **59** 2947

[3] Frey M T, Ling X, Lindsay B G, Smith K A and Dunning F B 1993 Use of the Stark effect to minimize residual electric fields in an experimental volume *Rev. Sci. Instrum.* **64** 3649

[4] Schramm A, Weber J M, Kreil J, Klar D, Ruf M-W and Hotop H 1998 Laser photoelectron attachment to molecules in a skimmed supersonic beam: diagnostics of weak electric fields and attachment cross sections down to 20 μeV *Phys. Rev. Lett.* **81** 778

[5] Osterwalder A and Merkt F 1999 Using high Rydberg states as electric field sensors *Phys. Rev. Lett.* **82** 1831

[6] Abel R P, Carr C, Krohn U and Adams C S 2011 Electrometry near a dielectric surface using Rydberg electromagnetically induced transparency *Phys. Rev.* A **84** 023408

[7] Bowden W, Hobson R, Huillery P, Gill P, Jones M P A and Hill I R 2017 Rydberg electrometry for optical lattice clocks *Phys. Rev.* A **96** 023419

[8] Sedlacek J A, Schwettmann A, Kübler H, Löw R, Pfau T and Shaffer J P 2012 Microwave electrometry with Rydberg atoms in a vapour cell using bright atomic resonances *Nat. Phys.* **8** 819

[9] Gordon J A, Holloway C L, Schwarzkopf A, Anderson D A, Miller S, Thaicharoen N and Raithel G 2014 Millimeter wave detection via Autler–Townes splitting in rubidium Rydberg atoms *Appl. Phys. Lett.* **105** 024104

[10] Zhelyazkova V and Hogan S D 2015 Probing interactions between Rydberg atoms with large electric dipole moments in amplitude-modulated electric fields *Phys. Rev.* A **92** 011402

[11] Zhelyazkova V and Hogan S D 2015 Rydberg-Stark states in oscillating electric fields *Mol. Phys.* **113** 3979

[12] Fan H, Kumar S, Sedlacek J, Kübler H, Karimkashi S and Shaffer J P 2015 Atom based RF electric field sensing *J. Phys. B: At. Mol. Opt. Phys.* **48** 202001

[13] Jiao Y, Han X, Yang Z, Li J, Raithel G, Zhao J and Jia S 2016 Spectroscopy of cesium Rydberg atoms in strong radio-frequency fields *Phys. Rev.* A **94** 023832

[14] Lutwak R, Holley J, Chang P P, Paine S, Kleppner D and Ducas T 1997 Circular states of atomic hydrogen *Phys. Rev.* A **56** 1443

[15] De Vries J C 2001 A precision millimeter-wave measurement of the Rydberg frequency *PhD Thesis* Massachusetts Institute of Technology

[16] Ramos A, Moore K and Raithel G 2017 Measuring the Rydberg constant using circular Rydberg atoms in an intensity-modulated optical lattice *Phys. Rev.* A **96** 032513

[17] Cassidy D 2018 Experimental progress in positronium laser physics *Eur. Phys. J.* D **72** 53

[18] Saffman M, Walker T G and Mølmer K 2010 Quantum information with Rydberg atoms *Rev. Mod. Phys.* **82** 2313

[19] Pohl R *et al* 2010 The size of the proton *Nature* **466** 213

[20] Pohl R, Gilman R, Miller G A and Pachucki K 2013 Muonic hydrogen and the proton radius puzzle *Annu. Rev. Nucl. Part. Sci.* **63** 175

[21] Carlson C E 2015 The proton radius puzzle *Prog. Part. Nucl. Phys.* **82** 59

[22] Beyer A *et al* 2017 The Rydberg constant and proton size from atomic hydrogen *Science* **358** 79

[23] Ye S, Zhang X, Killian T C, Dunning F B, Hiller M, Yoshida S, Nagele S and Burgdörfer J 2013 Production of very-high-*n* strontium Rydberg atoms *Phys. Rev.* A **88** 043430

[24] Schwartz H L, Miller T M and Bederson B 1974 Measurement of the static electric dipole polarizabilities of barium and strontium *Phys. Rev.* A **10** 1924

[25] Merkt F and Schmutz H 1998 Very high resolution spectroscopy of high Rydberg states of the argon atom *J. Chem. Phys.* **108** 10033

[26] Wörner H J, Hollenstein U and Merkt F 2003 Multichannel quantum defect theory and high-resolution spectroscopy of the hyperfine structure of high Rydberg states of ^{83}Kr *Phys. Rev.* A **68** 032510

[27] Schäfer M, Andrist M, Schmutz H, Lewen F, Winnewisser G and Merkt F 2006 A 240–380 GHz millimetre wave source for very high resolution spectroscopy of high Rydberg states *J. Phys. B: At. Mol. Opt. Phys.* **39** 831

[28] Mitroy J, Safronova M S and Clark C W 2010 Theory and applications of atomic and ionic polarizabilities *J. Phys. B: At. Mol. Opt. Phys.* **43** 202001

[29] Thiele T, Filipp S, Agner J A, Schmutz H, Deiglmayr J, Stammeier M, Allmendinger P, Merkt F and Wallraff A 2014 Manipulating Rydberg atoms close to surfaces at cryogenic temperatures *Phys. Rev.* A **90** 013414

[30] Halfmann T, Koensgen J and Bergmann K 2000 A source for a high-intensity pulsed beam of metastable helium atoms *Meas. Sci. Technol.* **11** 1510

[31] Zhelyazkova V, Jirschik R and Hogan S D 2016 Mean-field energy-level shifts and dielectric properties of strongly polarized Rydberg gases *Phys. Rev.* A **94** 053418

[32] Drake G W F and Morton D C 2007 A multiplet table for neutral helium (^{4}He I) with transition rates *Astrophys. J. Suppl. Ser.* **170** 251

[33] Drake G W F 1999 High precision theory of atomic helium *Phys. Scr.* **T83** 83

[34] Ahmadi M *et al* 2018 Characterization of the 1S–2S transition in antihydrogen *Nature* **557** 71